

Embedded disks around low-mass protostars

Eduard I. Vorobyov^{1,2} and Shantanu Basu³

¹ The Institute for Computational Astrophysics, Saint Mary's University, Halifax, Canada
email: vorobyov@ap.smu.ca

² Research Institute of Physics, Southern Federal University, Rostov-on-Don, Russia

³ The University of Western Ontario, London, Canada

Abstract. The time evolution of protostellar disks in the embedded phase of star formation (EPSF) is reviewed based on numerical hydrodynamics simulations of the gravitational collapse of two cloud cores with distinct initial masses. Special emphasis is given to disk, stellar, and envelope masses and also mass accretion rates onto the star. It is shown that accretion is highly variable in the EPSF, in agreement with recent theoretical and observational expectations. Protostellar disks quickly accumulate mass upon formation and may reach a sizeable fraction of the envelope mass ($\sim 35\%$) by the end of the Class 0 phase. Systems with disk-to-star mass ratio $\xi \approx 0.5$ are common but systems with $\xi \geq 1.0$ are rare because the latter quickly evolve into binary or multiple systems. Embedded disks are characterized by radial pulsations, the amplitude of which increases with growing core mass.

Keywords. accretion, accretion disks, (stars:) circumstellar matter, stars: formation.

1. Introduction

The embedded phase of the evolution of a protostellar disk, starting from its formation and ending with the clearing of a parent cloud core, set the course along which a young stellar object (YSO) will evolve later in the T Tauri phase. Despite its pivotal role, the embedded phase of star formation (EPSF) phase is poorly understood owing to difficulties with both observations and modeling. Directly observing disks in this phase is difficult as they are hidden within dense, extinguishing protostellar envelopes and only a handful of attempted studies exist (e.g. Jorgensen *et al.* 2009).

Self-consistent numerical simulations of protostellar disks in the EPSF are no less difficult than observations due to vastly changing spatial and temporal scales involved. The matter is that it is not sufficient to just consider an *isolated* system with some presumed disk-to-star mass ratio. A self-consistent treatment of the interaction of the star/disk system with the natal cloud core is of considerable importance for the disk physics and this inevitably requires solving for a much larger spatial volume than in isolated systems. Such multidimensional numerical simulations only recently have started to emerge (e.g. Vorobyov & Basu 2006, Vorobyov 2009a, and Attwood *et al.* 2009).

In this article, we make use of numerical hydrodynamics simulations in the thin-disk approximation to compute the gravitational collapse of rotating, gravitationally unstable cloud cores with an accurate treatment of disk thermodynamics. This allows us to realistically model the formation and long-term evolution of protostellar disks. The basic equations, initial conditions, and details of the code can be found in Vorobyov & Basu (2010).

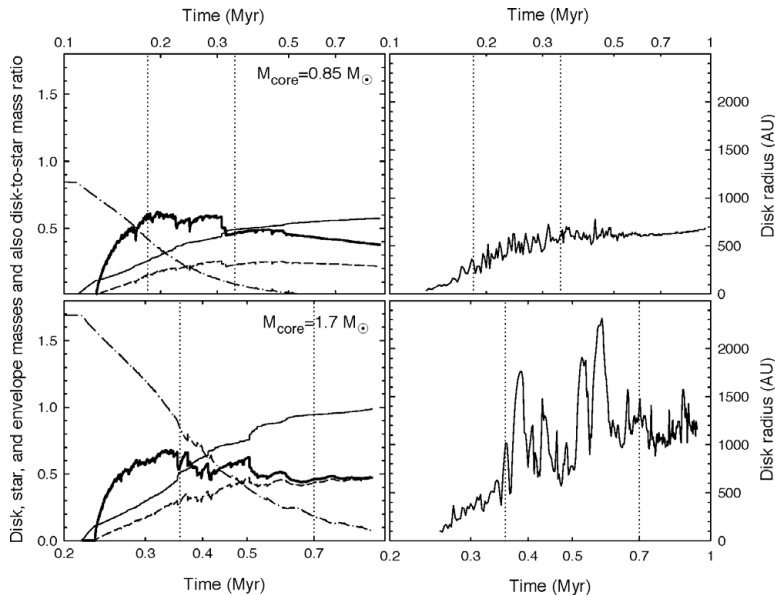


Figure 1. **Left column.** Time evolution of disk (dashed lines), envelope (dash-dotted lines), and stellar (thin solid lines) masses and also disk-to-star mass ratio (thick solid lines) in model 1 (top) and model 2 (bottom). **Right column.** Time evolution of disk outer radii in model 1 (top) and model 2 (bottom). The vertical dotted lines mark the onset of Class I (left) and Class II (right) phases of stellar evolution.

2. Time evolution of disk, stellar, and envelope masses

We start our numerical integration in the pre-stellar phase, which is characterized by a collapsing *starless* cloud core, continue into the embedded phase of star formation, during which a star, disk, and envelope are formed, and terminate our simulations in the T Tauri phase, when most of the envelope has accreted onto the forming star/disk system. In this section, we present results for two model cores with initial masses $M_{\text{core}} = 0.85 M_{\odot}$ (model 1) and $M_{\text{core}} = 1.7 M_{\odot}$ (model 2). The ratio of rotational to gravitational energy is $\beta = 5.6 \times 10^{-3}$. The left column in Figure 1 shows the time evolution of the stellar mass M_* (thin solid line), disk mass M_{d} (dashed line), envelope mass M_{env} (dash-dotted line), and disk-to-star mass ratio ξ (thick solid line) in model 1 (upper-left panel) and model 2 (lower-left panel). The separation of the burgeoning disk from the infalling envelope is done using a method described in detail in Vorobyov (2010), which is based on the typical transitional density $\Sigma_{\text{d2e}} = 0.1 \text{ g cm}^{-2}$ and the radial velocity field. The time is counted since the onset of core collapse. The vertical dotted lines mark the onset of the Class I (left) and Class II (right) phases of star formation as inferred from the total mass remaining in the envelope (André *et al.* 1993).

It is evident that by the end of the Class 0 phase the disk mass reaches a significant fraction of the envelope and stellar masses. For instance, in model 1 the disk-to-star mass ratio is $\xi = 0.59$ and the disk-to-envelope mass ratio is $\zeta = 0.37$, while in model 2 the corresponding values are $\xi = 0.56$ and $\zeta = 0.35$. Our simulations suggest that quite massive disks can be present as early as in the Class 0 phase, a conclusion that finds recent observational support (Enoch *et al.* 2009a).

Another interesting feature of Figure 1 is that the disk mass never exceeds that of the star, though ξ may become a substantial fraction of unity in the EPSF. It turns out that systems with $\xi \geq 1$ are unstable and quickly evolve via disk fragmentation into a

binary/multiple system. We therefore argue that such massive disks are feasible but they must be statistically rare.

The right column in Figure 1 depicts the time evolution of the disk outer radius in model 1 (upper right panel) and model 2 (lower-right panel). A remarkable feature of embedded disks is ongoing radial pulsations, the amplitude of which increases with growing core mass. These radial pulsations are caused by disk fragmentation and inward migration of massive fragments. The chain of events is as follows. Fragments form near corotation (most favourable place for fragmentation due to small shear) via fragmentation of dense spiral arms. These fragments interact gravitationally with the parent spiral arm and, as a result of this interaction, lose angular momentum and migrate radially inward. The disk expands in response to this migration to conserve the total angular momentum of the system. As a consequence, the gas surface density drops and the disk stabilizes temporarily until it contracts and accumulates enough mass from the infalling envelope for a next round of fragmentation to commence. Such radial pulsations continue as long as there is enough mass reservoir in the envelope (Class 0 and I phases), as Figure 1 suggests. In this sense, mass loading from the envelope can be regarded as the driving force of the radial pulsations but the actual disk expansion is caused by inward migration of the fragments.

3. Mass accretion history

The mass accretion history provides information on how stars accumulate mass and this may affect the internal structure and position of a star on the HR diagram (Baraffe *et al.* 2009). There is growing observational evidence that accretion onto a star is highly variable in the EPSF (e.g. Enoch *et al.* 2009b), in contrast to the theoretical predictions of the inside-out collapse (Shu 1977). Recent numerical simulations of polytropic protostellar disks by Vorobyov (2009b) have shown that the mass accretion rates \dot{M} in the Class I stage are expected to have a lognormal distribution, with its shape controlled by disk viscosity and disk temperature.

Our numerical modeling confirms that the accretion process onto the star is highly variable throughout much of the embedded phase. The top row in Figure 2 presents the mass accretion rates (in $M_{\odot} \text{ yr}^{-1}$) in model 1 (left panel) and model 2 (right panel) as a function of time. The vertical dotted lines mark the onset of the Class I (left) and Class II (right) phases of star formation. It is seen that \dot{M} in the EPSF exhibits short-term variations of several orders in magnitude, with the highest rates exceeding $10^{-4} M_{\odot} \text{ yr}^{-1}$ and lowest rates dropping below $10^{-9} M_{\odot} \text{ yr}^{-1}$. The bursts of high-rate accretion are caused by disk fragmentation. It turns out that most of the fragments spiral down onto the star due to the loss of angular momentum via gravitational interaction with spiral arms (Vorobyov & Basu 2006). On the other hand, an order of magnitude variability seen throughout much of the EPSF is caused by gravitational instability and non-linear interaction of low-order spiral modes. As shown by Vorobyov (2009b), this accretion flickering greatly reduces when disk self-gravity is artificially turned off, confirming that the disk gravitational destabilization lies behind this effect.

The highly variable accretion makes the star sporadically increase its *total* luminosity, as illustrated in the bottom panel of Figure 2. The solid lines present the accretion luminosity L_{accr} , while the red dashed lines depict the photospheric luminosity L_{ph} . Several clear-cut luminosity outbursts with L_{accr} as high as $100 L_{\odot}$ and many more weaker bursts (solid line) are evident against the background of a near-constant photospheric luminosity with $L_{\text{ph}} \sim 1.0 L_{\odot}$ (dashed line). The stronger bursts may represent FU Orionis-like eruptions, while weaker ones may manifest EX Lupi-like eruptions (EXOrs).

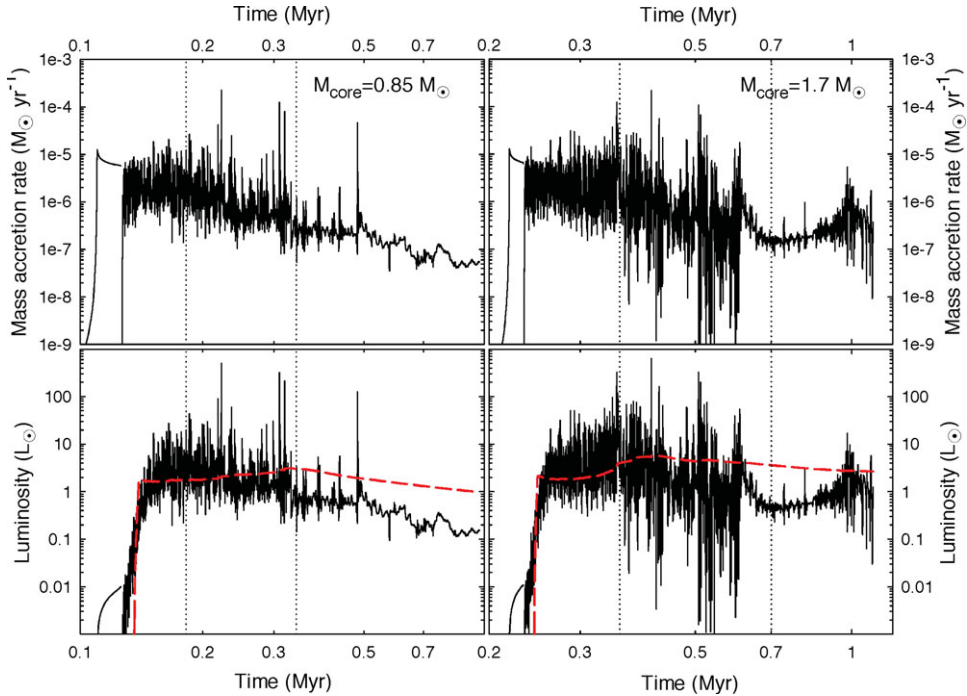


Figure 2. **Top row.** Mass accretion rate onto the star as a function of time in model 1 (left) and model 2 (right). **Bottom row.** Photospheric (red dashed lines) and accretion (solid lines) luminosity in model 1 (left) and model 2 (right). Vertical dotted lines mark the onset of Class I (left) and Class II (right) phases.

Acknowledgements

The authors thank the anonymous referee for useful comments. E.I.V. gratefully acknowledges present support from an ACEnet Fellowship, RFBR grant 10-02-00278, and Ministry of Education grant RNP 2.1.1/1937. Numerical simulations were done on the Atlantic Computational Excellence Network (ACEnet), on the Shared Hierarchical Academic Research Computing Network (SHARCNET), and at the Center of Collective Supercomputer Resources, Taganrog Technological Institute. S. B. was supported by a Discovery Grant from the Natural Sciences and Engineering Research Council of Canada.

References

- André, P., Ward-Thompson, D., & Barsony, M. 1993, *ApJ*, 406, 122
 Attwood, R. E., Goodwin, S. P., Stamatellos, D., Whitworth, A. P. 2009, *A&A*, 495, 201
 Baraffe, I., Chabrier, G., & Gallardo, J. 2009, *ApJ* (Letters), 702, 27
 Enoch, M. L., Corder, S., Dunham, M. M., & Duchéne, G. 2009, *ApJ*, 707, 103
 Enoch, M. L., Evans, N. J., II, Sargent, A. I., & Glenn, J. 2009, *ApJ*, 692, 973
 Jørgensen, J. K., van Dishoeck, E. F., Visser, R., Bourke, T. L., Wilner, D. J., Lommen, D., Hogerheijde, M. R., & Myers, P. C. 2009, *A&A*, 507, 861
 Shu, F. H. 1977, *ApJ*, 214, 488
 Vorobyov, E. I. & Basu, S. 2006, *ApJ*, 650, 956
 Vorobyov, E. I., 2009a, *ApJ*, 692, 1609
 Vorobyov, E. I. 2009b, *ApJ*, 704, 715
 Vorobyov, E. I. 2010, *ApJ*, 713, 1
 Vorobyov, E. I. & Basu, S. 2010, *ApJ*, 719, 1896